Research Article Vol. 1, No. 9 / 15 Sep 2022 / Optics Continuum 2077
OPTICS CONTINUUM

Power consumption analysis of an optical modulator based on different amounts of graphene

DANIEL NEVES,[1] RAFAEL NOBREGA,[2] ANDERSON SANCHES,[2] ANTONIO JURADO-NAVAS,[3] IVAN GLESK,[4] SHYQYRI HAXHA,[5] AND THIAGO RADDO[2,3,*]

[1]*Electrical Engineering Department, Federal University of Ceara, Sobral, Ceara, Brazil*
[2]*Engineering, Modeling & Applied Social Sciences Center, Federal University of ABC, Brazil*
[3]*Telecommunication Research Institute, University of Malaga, Malaga, Spain*
[4]*Faculty of Engineering, University of Strathclyde, Glasgow, United Kingdom*
[5]*Department of Electronic Engineering, Royal Holloway, University of London, United Kingdom*
[*]*thiago@ic.uma.es*

Abstract: Energy-efficient devices will play a key role in the continued performance scaling of next-generation information and communications technology systems. Graphene has emerged as a key optoelectronic material with unique energy-like properties. But to the best of our knowledge, these advantages have not yet been fully exploited in optical modulators design. In this work, we design and analyze an optical modulator which is composed of two graphene layers and a ring resonator made with different amount of graphene. For performance analysis, the ring resonator's amount of graphene is varied from 25 to 100% with four discrete steps. The critical coupling condition representing the OFF-state, and the 3-dB transmission level representing the ON-state of the device are obtained. Numerical results show this new optical modulator consumes as little energy as 4.6 fJ/bit whilst achieving a high-speed operation with a bandwidth up to 42.6 GHz when employing surprisingly only 25% of graphene. The 42.6 GHz modulator has a footprint as small as 22.1 μm^2 with an active area of 1.68 μm^2 only, the smallest active area to date. Alternatively, the optical modulator achieves up to ~88.5 GHz at the expense of consuming 17.5 fJ/bit when using 100% of graphene. The proposed graphene-based modulator proved to be a compact, energy-efficient, high-speed device, useful for a myriad of applications including mobile fronthaul, telecom, and datacom.

1. Introduction

Currently, there is a rapid deployment of deep optical fibre in many countries as a direct result of the rollout of the fifth-generation mobile systems [1]. The deep fibre deployment provides connectivity mainly between central offices and remote radio head antennas [2]. This network segment, called mobile fronthaul, will be eventually based on millimeter wave spectrum technologies supporting higher bandwidth and data rates whilst coping with challenging energy consumption requirements [3]. This growing uptake of the mobile fronthaul based on optical fibers is expected to enable a new range of emerging applications, not yet fully mature and commercially available, which may further push energy consumption beyond unexpected levels. The power consumption is becoming a concern in terms of energy costs and carbon dioxide emissions. Therefore, energy-efficient information and communications technology (ICT) will underlie a key role in performance progress scaling and also to limit increasing environmental impacts. Continuous improvements in the energy efficiency and power consumption of ICT equipment to significantly reduce carbon dioxide emissions by utilizing greener technologies has

#462268 https://doi.org/10.1364/OPTCON.462268
Journal © 2022 Received 29 Apr 2022; revised 5 Aug 2022; accepted 10 Aug 2022; published 15 Sep 2022

OPTICS CONTINUUM

become of major importance [4–6]. Current technologies still face challenges not only to meet energy-per-bit requirements, but also bandwidth, footprint and cost.

Graphene, a CMOS compatible technology with a single layer of carbon atoms, has many unique characteristics. These include high thermal stability, tunable conductivity, and ultra-high carrier mobility. Among several technologies regarded as greener, graphene has been successfully proven relevant for ICT building blocks such as optical modulators [7,8]. A graphene-based modulator was first demonstrated a decade ago [9]. Since then, several graphene-based modulators have been proposed [10–31]. Optical modulators based on graphene have outperformed traditional modulators in terms of the bandwidth, power consumption, and footprint. For example, several works have addressed the performance of graphene-based modulators [9,14,22,24,28]. However, they still have room for performance improvements, especially in the power consumption, bandwidth, and footprint.

In this paper, we propose a new design based on the graphene's amount of an optical modulator and then analyze its power consumption. The new design reduces the power consumption of the optical modulator below 5 fJ per bit. The modulator consists of two graphene layers, an alumina layer, and a ring resonator. The latter is partially made with different amount of graphene. The amount of graphene on the ring resonator is varied from 25% to 100% with four discrete steps for analysis. For example, 25% graphene modulator means the ring resonator is only partially covered with graphene. The chemical potential is obtained to the OFF-state as a key parameter to yield distinct characteristics in the device's behavior and operation. The critical coupling condition representing the OFF-state, and the 3-dB transmission level representing the ON-state are obtained for the analysis. The parameters of the modulator are extracted based on transmission characteristics by using the finite element technique. Numerical results show the new graphene modulator consumes as little energy as 4.6 fJ/bit whilst achieving high-speed operation with bandwidth of 42.6 GHz. This modulator's performance is a significant achievement as only 25% of its ring resonator area is covered with graphene, providing a substantial cost reduction when compared to traditional graphene modulators. Alternatively, the modulator operates at up to ~88.5 GHz whilst still within femtojoule levels of power consumption (17.5 fJ/bit), but with 100% of graphene. Finally, the 42.6 GHz modulator has a footprint as small as 22.1 μm^2 with an active area of only 1.68 μm^2. To the best of our knowledge, this is the smallest active area to date. This renders graphene-based modulators to be energy-efficient, high-speed, compact and useful for myriad of applications within ICT including mobile fronthaul, telecom, and datacom.

2. Graphene and its optical and electrical properties

The physical understanding of graphene's optoelectronic properties are of great interest for ICT applications. Graphene allows its electrons close to the k point to have zero effective mass by presenting an energy curve of linear dispersion. This renders the material with high charge mobility and extremely sensitive to its optical properties variations, which can be achieved with small variations in the level of their chemical potential, whether achieved via chemical interaction with other molecules or atoms, or via application of an external electric field, changing their dielectric and optical absorption properties [7].

A- Graphene Optical Conductivity

Fermi level lies close to the Dirac point due to gapless band property of graphene. Hence, maximum amount of the incident photon energy is absorbed by the valence band electron to make inter-band transition and thus the optical transmission through the modulator decreases. Accordingly, both inter-band and intra-band transition that determine the complex optical

OPTICS CONTINUUM

conductivity of graphene can be expressed by using the Kubo's integral as follows [32]

$$\sigma(\mu,\omega,T,\Gamma)_{total} = \frac{je^2(\omega - j2\Gamma)}{\pi\hbar^2} \left[\frac{1}{(\omega - 2j\Gamma)^2} \int_0^\infty \varepsilon \left(\frac{\partial f_d(\varepsilon,\mu)}{\partial\varepsilon} - \frac{\partial f_d(-\varepsilon,\mu)}{\partial\varepsilon} \right) d\varepsilon - \int_0^\infty \frac{f_d(-\varepsilon,\mu) - f_d(\varepsilon,\mu)}{(\omega - 2j\Gamma)^2 - 4\left(\frac{\varepsilon}{\hbar}\right)^2} d\varepsilon \right]. \quad (1)$$

Where $f_d(\varepsilon,\mu) = [e^{(\varepsilon-\mu)/k_BT} + 1]^{-1}$ f_d (ε,μ) represents the Fermi distribution of states with energy ε, μ is the chemical potential in electron-volt, ω is the angular frequency, T is the absolute temperature in Kelvin and Γ represents the scattering rate of charged particles. Accordingly, it is possible to obtain by solving this integral the expression that gives us the permittivity of the graphene sheet with thickness Δ in terms of its real (σ_{real}) and imaginary σ_{im} parts of conductivity as

$$\varepsilon_{rgraph} = 1 - \frac{\sigma_{im}}{\Delta\omega} + j\frac{\sigma_{real}}{\Delta\omega}. \quad (2)$$

B- Critical Coupling of the All-pass Resonator

Let us assume an all-pass resonator coupling to bus waveguide. Then, according to the critical coupling theory [33], the scattering matrix that represents the coupling can be obtained as

$$(b_1\ b_2\ ) = (tk\ \ -k^*t^*\ )(a_1\ a_2\ ), \quad (3)$$

t, k, a_1 *and* b_1 represent the transmission, coupling, input and output coefficients respectively and $\boldsymbol{a}_2 = \boldsymbol{b}_2\sigma\ e^{j\theta}$ where θ represents the resonator phase. Given the circulation condition inside the resonator, where α and θ represent the round trip loss coefficient and the phase shift angle, respectively. Thus, the expression for the ratio of transmitted output and input power can be calculated as follows

$$T = \left|\frac{b_1}{a_1}\right|^2 = |b_1|^2 = \frac{\alpha^2 + |t|^2 - 2\alpha|t|cos(\theta)}{1 + \alpha^2|t|^2 - 2\alpha|t|cos(\theta)}. \quad (4)$$

Interestingly, this equation allows someone to address the variation in the transmission proprieties due to both absorption and phase effects. Accordingly, when graphene is used as the active material, its real and imaginary conductivity are related to the losses and phase shift.

3. Design and properties of the optical modulator

This section describes in detail the structure design and proprieties that ate common for the optical modulator investigated in this work. Comsol Multiphysics 3.5a has been used for this numerical analysis. Accordingly, the structure of the modulator, shown in Fig. 1, is based on a silicon (Si) core bus waveguide of width $W_1 = 340$ nm coupled to a ring-shaped silicon resonator whose width is fixed as $W_2 = 600$ nm in which both core silicon waveguides have the same thickness $h_{Si} = 220$ nm. Moreover, on top of the silicon core, the resonator is partially covered with three thin layers. The first layer is composed of graphene and has thickness $h_g = 0.34$ nm, the second layer is composed of alumina with thickness $h_a = 7$ nm, and finally the top layer is also made of graphene with the same thickness $h_g = 0.34$ nm. The entire structure is surrounded by silica substrate. It is worth point out that this kind of double-layer structure has smaller formfactor than single-layer designs, being favorable for further device footprint reduction [18]. Furthermore, since the optical and electrical response of graphene is much faster than in doped silicon, it reduces the bandwidth limitation related to the rise and relaxation lifetime of the free carrier concentrations [9,13]. Lastly, there are two metal contacts on the top of the silica substrate with each connected to a graphene layer, forming a capacitor. The two metal electrodes are placed accordingly so as the losses become negligible but not too far from the waveguides in order

OPTICS CONTINUUM

to mitigate the contribution of sheet resistance as in [9,15,24]. The described device can be fabricated, for example, with chemical vapor deposition grown graphene sandwiched between silicon and silica substrate, followed by a photolithography and etching. For all simulations, a quasi-TE fundamental mode is excited at the input port 1 as it provides a better confinement than does the fundamental quasi-TM mode. It is worth mentioning that the values defined for W_1 and W_2 have been optimized in order to maximize their efficiency in terms of gap considering the fabrication feasibility and to minimize bending losses for resonators with external radius of 2.08 µm whilst still preserving a fundamental mode resonant structure. Judicious design and optimization of these parameters might enable unique advantages within graphene proprieties, giving rise to overall performance improvements. The analysis and results for this optimization procedure are shown in Fig. 2(a), b. In this fashion, from the dispersion curves of the resonant wavelength for the first and second order radial modes plotted in Fig. 2(a), we can establish the cut-off width $W_2 = 600$ nm, for which the first order radial mode interacts weakly with the inner sidewalls whereas the second order mode is completely suppressed. This effect can be clearly seen for the cross-sectional mode profile considering the electrical field provided in Fig. 2(a) for different resonator widths. Regarding the W_1 optimization, our simulations show that for a waveguide width smaller than 340 nm is possible to reach a wider gap for the critical coupling tunning which is less sensitive to fabrication errors (see Fig. 2(b)). It is worth to pointing out that the waveguide supports single mode operations even for widths smaller than 340 nm. Furthermore, it is noteworthy that the effect of free charges transfers from the graphene layer to the silicon waveguide due to the direct contact between both surfaces, is neglected. The latter is due to the coefficient value of the TE mode (-8.72×10^4 dB/µm/mW) [34], which is one order of magnitude lower than does the bending losses of the resonator, considering low coupled power of 0.5 mW and an external radius of 2.08 µm. It should be further noted that the loss related to the ring's curvature as well as the graphene optical absorption are taken into account for the

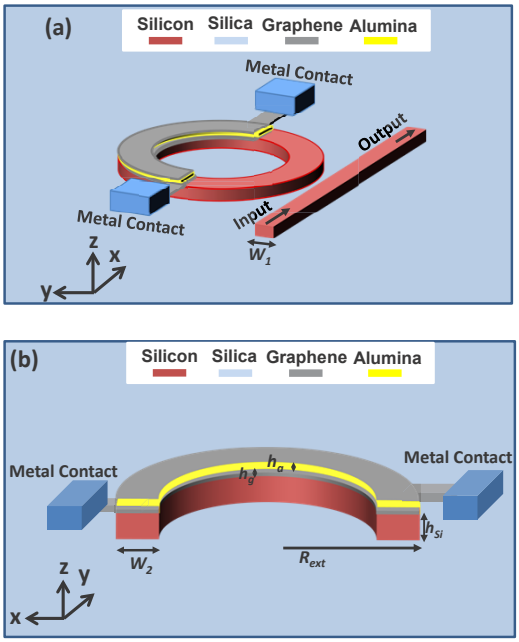

Fig. 1. (a) Front-view of a graphene ring-resonator coupled with a bus waveguide (width W_1); (b) Cross-sectional view of the modulator. W_2 is ring waveguide width, *Rext* is the ring external radius, and *hg* and *ha* are the thickness of graphene and alumina layers, respectively.

OPTICS CONTINUUM

device's optimization by considering gap values satisfying the modulator's critical coupling condition. Moreover, the graphene's permittivity is obtained via the Kubo's formula [32], by substituting the results of its conductivity (for $T = 300$ K and $\Gamma = 0.43$ meV) into (2). Finally, we use the experimental values obtained from [35–37] for the refractive indexes of silicon, silica and alumina.

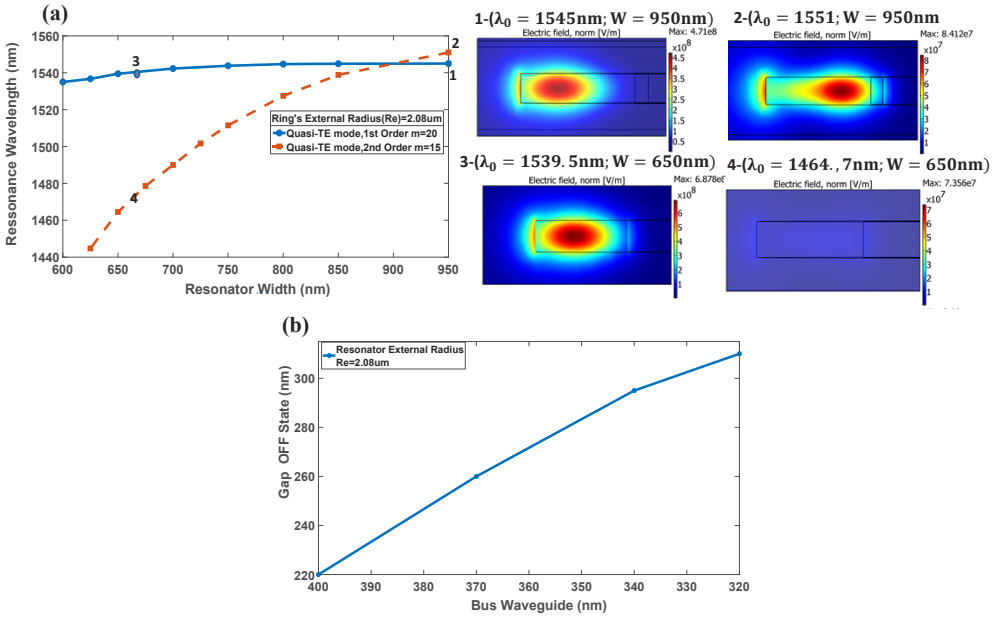

Fig. 2. (a) Dispersion curves of resonance wavelength of the first (blue line) and second (red line) order radial modes as a function of the resonator width (W_2); (b) OFF state gap as a function of the bus waveguide width (W_1).

4. Performance analysis of the graphene-based optical modulator

This section discusses the chemical potential properties of the modulator, simulation methodology, and the optimization of the resonator. Once we have defined the main features, the analysis of the functionality and behavior of the modulator including the ON- and OFF-states can be addressed in the next step. It is worth mentioning that 3D simulations are carried out with the help of an approximation methodology as the direct computational cost with all layers included would be prohibitive. Accordingly, without loss of generality and accuracy, the homogenization approximation of the transverse structure of the waveguide is defined as follows: both layers of graphene and the layer of alumina are replaced for device's benchmark purposes only by a homogeneous waveguide with index of refraction n_{homog} given by as

$$n_{homog.} = n_{Si} + \alpha(\mu, \lambda) + j\beta(\mu, \lambda), \tag{5}$$

and

$$neff_{graphene} = neff_{homog.} \tag{6}$$

where α and β are the real and imaginary parts of the silicon refractive index being a function of the wavelength and chemical potential. n_{Si} is the silicon refractive index, and $neff_{homog}$ and $neff_{graphene}$ are the effective refractive index of the homogeneous and graphene-assisted waveguides, respectively. Accordingly, (5) and (6) render a homogeneous waveguide instead of

OPTICS CONTINUUM

a classical heterogeneous waveguide with different index of refraction values. For the method proposed here, the error estimation is stipulated in terms of both, variation of the real and imaginary part of the refractive index. The estimated error for both refractive indexes is ~0.05% only. This means that the method accounts for the graphene's behavior based on variation of phase and losses (i.e., by considering the real and imaginary parts, Δneff) for ON- and OFF-states. It is worth pointing out that the proposed homogeneous approximation renders the key advantage of being computationally faster and more efficient model for performance benchmarking of the graphene-based device.

Next, we analyze the chemical potential properties of the modulator considering different quantities of graphene. A schematic illustration of the waveguide homogenization technique is depicted in detail in Fig. 3(a). The variation of the real and imaginary part of index versus the chemical potential for a wavelength of 1.5344 μm is plotted in Fig. 3(b). Let us to consider the modulator (amplitude and phase modulation), then, the chemical potential for its OFF-state is 0.444 eV. The latter represents the highest value obtained from the optimal variation range of the graphene's real and imaginary conductivity (see Fig. 3(b)). It is worth mentioning that the analysis considers that both graphene layers are simultaneously at the same chemical potential. Moreover, the initial doping of both graphene layers is taken into account, which is near −0.125 eV associated along with $n = 1.1 \times 10^{12}\,\mathrm{cm}^2$ [38]. Then, the applied gate voltage of 2.05 V leads to a slightly asymmetric chemical potential in both graphene layers, which means that one layer is at −0.459 eV and the other layer is at 0.4285 eV. This corresponds to a deviation of the 0.444 eV in both layers in a way that one layer has a higher doping level (increase by $\sim 1.1 \times 10^{12}\,\mathrm{cm}^2$) whereas the second layer has a lower doping level (decrease by $\sim 1.1 \times 10^{12}\,\mathrm{cm}^2$). Accordingly, this proportional loss compensation makes the asymmetry effect negligible as in [24,38], and consequently both layers have the same chemical potential. Remarkably, this allows to maximize both the modulator optical absorption's and phase variation ratio which is beneficial to reduce the modulator's power consumption. For the sake of conciseness, the dependence of the chemical potentials as a function of the applied gate voltage, taking into account the natural doping level of graphene represented by a given offset potential, can be depicted as

$$\mu_c = \hbar v_f \sqrt{\pi \left(e \left(\frac{\varepsilon_0 \varepsilon_{r,diel.}}{h_{diel.}} \right) (\mathrm{V} + V_0) \right)}. \tag{7}$$

Where v_f stands for fermi velocity, $\hbar$ for modified Planck constant, V is the gate voltage and V_0 is the voltage offset caused by graphene's natural doping, and e is electron charge, and $\left(\frac{\varepsilon_0 \varepsilon_{r,diel.}}{h_{diel.}} \right)$ is the capacitance per unit area. It is noteworthy that the applied voltage induces a p-type in one and n-type in the other graphene layer i.e., representing the same chemical potential level.

The ON-state of the modulator is obtained for a level of chemical potential in which the insertion loss of −3 dB is considered. The same resonance wavelength is used as for the OFF-state. Then, this analysis is carried out many times by varying the ring's amount of graphene from 25% to 100% within four discrete steps (25%, 50%, 75%, and 100%) while considering the ring external radius of 2.08 μm. At the resonance wavelength of 1,534.4 nm and the external radius of 2.08 um and graphene and alumina layers of 0.34 nm and 7 nm, respectively, the maximum modulation depth of 27 dB is demonstrated. The experimental characterization of the proposed device along with its validation will be addressed as future work. The unloaded quality (Q) factor of the microring resonator is 13.820, which is obtained considering the optical bandwidth in its critical coupling condition (gap = 295 nm). Moreover, the Q factor values are 4213.1, 2488.2, 1743.8, and 1310.4 for 25%, 50%, 75% and 100% graphene. These values are calculated based on our simulations. Next, we carry out the analysis of the graphene modulator properties, including the losses. It is noteworthy to mention that the total losses of the device are related to

OPTICS CONTINUUM

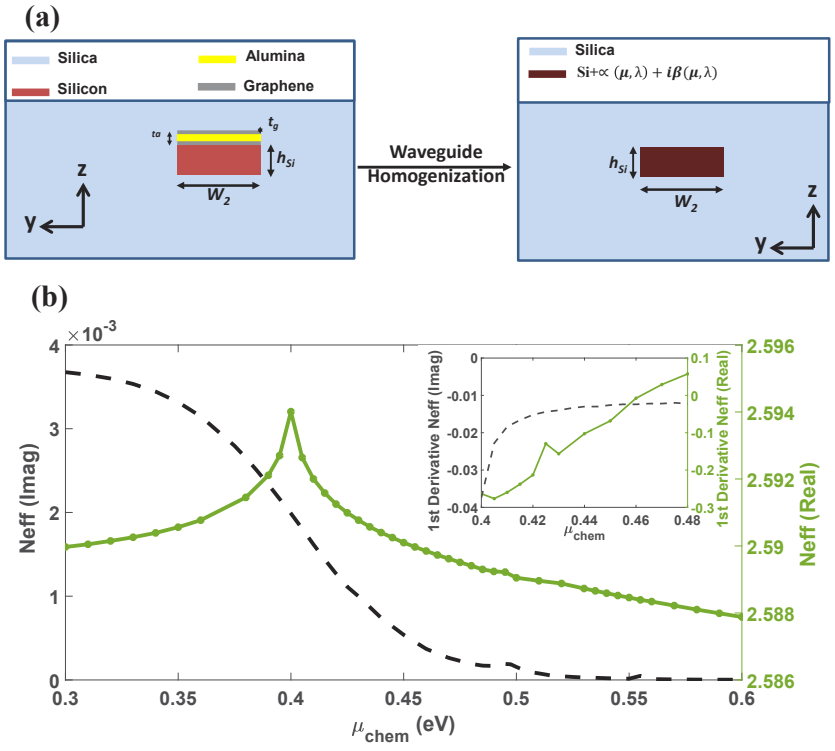

Fig. 3. (a) Schematic representation of the homogenization approximation technique for the resonator waveguide; (b) Real (orange) and imaginary (blue) part of the effective index for the graphene modulator with $W_2 = 600$ nm, $h_{Si} = 220$ nm, $h_g = 0.34$ nm, $h_a = 7$ nm, and $\lambda = 1{,}534.4$ nm. **Inset**: first derivative of real (green) and imaginary (black) part of the refractive index considering a chemical potential (μ_{chem}) interval between 0.4 - 0.48 eV.

the bandwidth BW when the critical coupling ($\alpha = t$). The BW is given by [39]

$$BW_{-3dB}(nm) = \frac{(1-\alpha^2)\lambda_0^2}{2\pi^2 R n_g \alpha}, \tag{8}$$

where n_g, R, and λ_0, are the group index, mean radius, and resonance wavelength of the resonator for the propagated mode. The results obtained for the aforementioned analysis are listed in Table 1. It is considered the same criterion of insertion loss for the ON-state (−3 dB) and identical external radius for different amounts of graphene's ring percentage. Next the numerical simulations for different configurations of the modulator are performed. By using the values obtained for the chemical potential for each graphene amount, the power consumption per bit (Joules/bit) as [13], in which $\rho_{on} > \rho_{off}$,

$$E_{J/bit} = \frac{1}{2}\frac{(Q^2{}_{ON} - Q^2{}_{OFF})}{2C} = \frac{1}{4}(\rho^2{}_{ON} - \rho^2{}_{OFF})e^2\ \frac{h_{diel.}\,S}{\varepsilon_0 \varepsilon_r}, \tag{9}$$

where Q_{ON} and Q_{OFF} represent the amount of charge that correspond to the on and OFF state, respectively, C is the modulator's capacitance, ρ_{on} *and* ρ_{off} are the carrier concentrations for the graphene's chemical potential equivalent to the ON and OFF states, e is the electron charge, $h_{dielectric}$ is the dielectric thickness, ε_0 and ε_r are the vacuum and relative permittivity, respectively, and S represents the capacitor's area, which corresponds to the area on the top

OPTICS CONTINUUM

surface of the resonator. Afterwards, we measured the −3 dB bandwidth. It is also possible to define the figure-of-merit (FOM) [40] of the modulator as follows

$$FOM = \frac{FWHM(GHz)}{[Power\ Comsumption(E/bit)\ X\ Area(um^2)]}, \tag{10}$$

where *FWHM* is the full width at half-maximum pulse in the frequency domain, *E* is the energy required for switching, and *Power Consumption* and *Area* are the power-per-bit consumption and full area of the device, respectively. Having a FOM provides an expression representing the device efficiency i.e., gauging its performance. This is very useful for its optimization and predicting the expected behavior of its design for a given configuration.

Table 1. Simulation Parameters

Graphene (%)	Total Loss OFF-State dB/μm)	OFF-State Gap (nm)	Chemical Potential OFF (eV)	Chemical Potential ON (eV)
25	−0.0089	205	0.444	0.4095
50	−0.0150	170	0.444	0.4115
75	−0.0214	145	0.444	0.4115
100	−0.0245	125	0.444	0.4115

5. Simulation results

The performance of the new graphene ring resonator coupled with a bus waveguide is now analyzed for four distinct amounts of graphene 25%, 50%, 75%, and 100%. The aim is to obtain the device maximum efficiency in terms of power consumption per bit. It becomes helpful to recall the resonator's configuration before proceeding with the modulator's analysis itself. The modulator has a radius with dimension of 2.08 μm covered with a graphene and alumina layer of 0.34 nm and 7 nm, respectively. For the first configuration, the value of the chemical potential for its OFF state equals to 0.444 eV was chosen to maximize the optical absorption's variation ratio. In this case, the ON state was obtained for a level of chemical potential equivalent to an insertion loss of −3 dB. It is worth pointing out that, without any loss of generality or accuracy, the device structure can be considered as two graphene layers having the same chemical potential due to the gate voltage level utilized, which takes the chemical potential to be equally distributed in both graphene layers [24,38,41–43]. Once the relevant device parameters have been adequately described, the performance can be discussed.

Initially, we carry out the analysis of the graphene modulator properties considering the transmission parameter (S_{21}). The transmission parameter versus the wavelength by considering both, OFF- and ON-states and the four percentages of graphene is plotted in Fig. 4. This figure schematically shows the power transferred from port 1 to port 2 that is given by the S_{21} parameter as part of the tuning procedure of the modulator in its OFF (red curve) and ON (blue curve) states. The adjustment of the critical coupling is carried out according to the gap variation between the bus and the resonator. One can observe that both curves (red and blue) have a minor displacement of the propagation wavelength towards higher values which is due insignificant phase variation in comparison to the propagation wavelength. This happens due to the device's coupling propagation region being much smaller than the beat length. On one hand, the real part of the graphene's dielectric constant is responsible for the phase variation of the resonator that changes the confined mode resonance condition. On the other hand, the imaginary part of the dielectric constant is responsible for changing the resonator loss coefficient which, in turn, changes the power transmitted from port 1 to port 2, since it 'shifts' the bus resonator from its critical coupling condition. As the consequence, one can note a displacement of the resonance

OPTICS CONTINUUM

valley and transmission value. Finally, the extinction ratios are −34.27 dB, −39.13 dB, 51.52 dB, and 32.26 dB for 25%, 50%, 75% and 100% graphene, respectively. Next, it is investigated the chemical potential ON-OFF variation as a function of the percentage of graphene's ring percentage. The results are plotted in Fig. 5(a) (orange). These results give important evidences on how much graphene should be used.

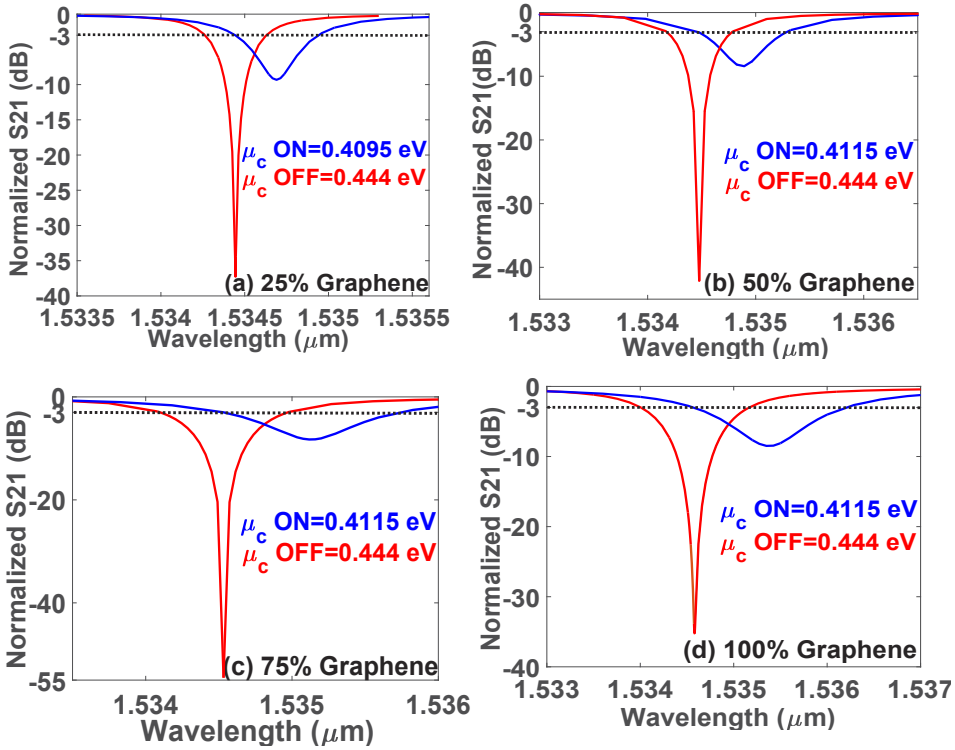

Fig. 4. The modulator's transmission curves versus the wavelength considering both OFF (red) and ON (blue) states and different percentages of graphene. (a) 25% graphene, (b) 50% graphene, (c) 75% graphene, and (d) 100% graphene.

As can be observed, the modulator shows decrease in the chemical potential ON-OFF variation as a function of the graphene ring percentage. The device must be able to perform high-speed switching. Thus, bandwidth characteristics supported by the modulator will be investigated. The −3 dB bandwidth as a function of the levels of graphene's ring percentage is plotted in Fig. 5(b) (blue). Results show that the bandwidth increases significantly with the graphene ring percentage. This occurs due to increases of graphene-related losses as the graphene percentage is increased. Consequently, the modulator can offer ultra-high switching properties if higher percentages of graphene are used. Table 2 summarizes the main modulator parameters (ON- and OFF-states, total losses, ON and OFF chemical potentials) as well as its figures-of-merit (bandwidth, power consumption per bit, trade-off benchmark) considering four discrete amount of graphene (25, 50, 75 and 100%). The value of f_{RC} = 110 GHz, regardless of the device's active area. Nonetheless, the value of R and C change with the given active area. For example, for an active area of 1.68 um^2 (25% of graphene) R = 71.54 Ω and C = 20.26 fF, for 3.36 um^2 (50% graphene) R = 35.77 Ω and C = 40.52 fF, for 5.04 um^2 (75% graphene) R = 23.84 Ω and C = 60.78 fF, and for 6.72 um^2 (100% graphene) R = 17.88 Ω and C = 81.04 fF, respectively. The modulator's contact resistance is 100 Ω.μm considering nickel as the contact electrode. Notice that for 50% of graphene the

OPTICS CONTINUUM

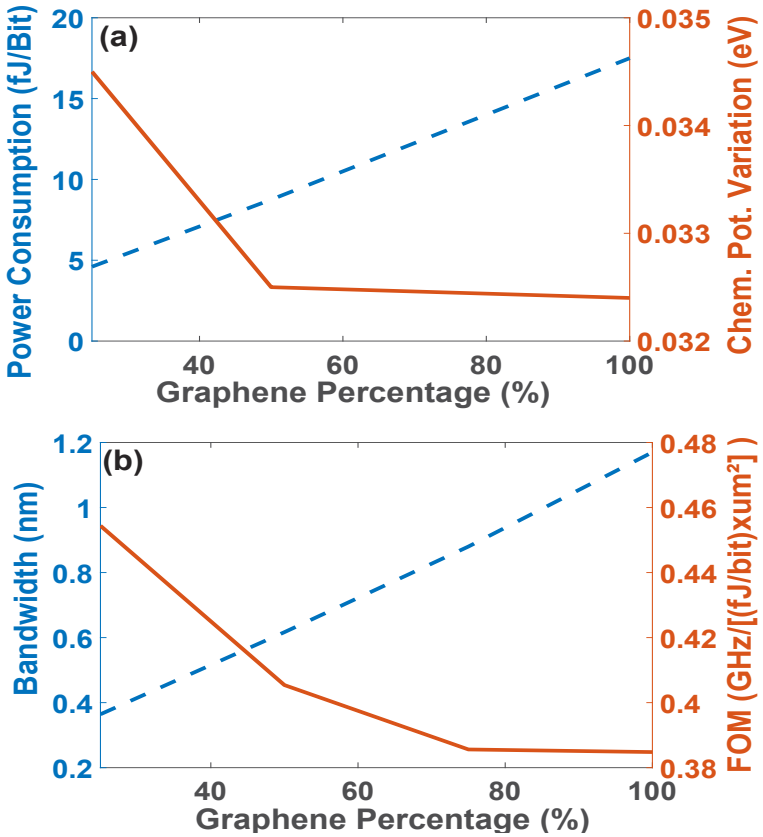

Fig. 5. Modulator's performance. (a) power consumption per bit (blue) and chemical potential ON-OFF variation (orange); (b) −3 dB bandwidth (blue) and trade-off performance efficiency (orange) as function of the graphene's ring percentage.

Table 2. Comparison of the modulator performance for different percentage of graphene

Graphene (%)	25	50	75	100
μ_{off} (eV)	0.444	0.444	0.444	0.444
μ_{on} (eV)	0.4095	0.4115	0.4115	0.4115
f_{opt} (GHz)	46.3	78.3	111.8	148.8
f_{RC} (GHz)	110	110	110	110
f_{3dB} (GHz)	42.67	63.81	78.41	88.45
E/bit (fJ/bit)	4.6	8.75	13.1	17.5
$Loss$ (dB/μm)	−0.0089	−0.015	−0.0214	0.0285
FOM_{3dB} (GHz/(fJ x μm^2)	0.4184	0.3302	0.2704	0.2287

OPTICS CONTINUUM

modulator offers a large bandwidth (78.3 GHz) with power consumption below 10 fJ per bit. For 25% of graphene, the modulator has an active area of 1.68 μm^2 whereas with 100% graphene, the modulator occupies 6.72 μm^2. This means an effective 4-fold reduction of the modulator active area. With the size, there is also a substantial cost reduction. High-quality graphene is still very expensive. Hence, the amount of graphene used in the design has a direct impact on the device's final cost. Accordingly, the 25% graphene modulator might be 4-fold cheaper than the 100% graphene modulator regarding the graphene.

Table 3. Comparison on performance metrics of graphene-based modulators

Modulator Type	Ref	f_{3dB} (GHz)	Footprint (μm^2)	Energy Consumption (fJ/bit)	FOM (GHz/fJbit×um^2)	Active area (um^2)
Multi-layer Graphene	[44]	3.6	96	10	3.75×10^{-3}	96
Double-layer Graphene	[45]	7.5	117.8	188	3.39×10^{-4}	82.1
Double-layer Graphene	[24]	10	20	2000	2.5×10^{-5}	20
Graphene-based WG	[18]	34	55	4.26	1.14×10^{-1}	55
Graphene-based Ring	[22]	285.5	8.9	33.6	9.6×10^{-1}	3.5
25% Graphene-based Ring	This work	42.6	22.1	4.6	4.18×10^{-1}	1.68
100% Graphene-based Ring	This work	88.45	22.1	17.5	2.23×10^{-1}	6.72

Lastly, the performance efficiency of the modulator as a function of the graphene's ring percentage is investigated. These results are shown in Fig. 5(b) (orange). It is also essential to evaluate the trade-off between the bandwidth and the power consumption and the device's footprint since such parameters have opposite contributions to the overall modulator performance. Notice that the overall performance deteriorates by increasing the ring's graphene percentage. In this case, the reduction of the active resonator area through the increases of the graphene in ring widening percentage implies a significant reduction in the device efficiency. This occurs because the large bandwidth obtained by the increasing graphene ring effect is compensated by the deleterious effect that of the high-power consumption per bit. This suggests that if the main goal of the device optimization is to minimize its overall power consumption, is worthwhile to limit the amount of graphene to one-quarter of the whole resonator but doing so the bandwidth is reduced. If this approach is implemented, such a device can be built to fit an extremely small area of 22.1 μm^2 and still offering a wide bandwidth of 42.6 GHz with very low levels of power consumption just as 4.6 fJ/bit. The performance in terms of modulation depth and bandwidth can be boosted if the entire resonator area is covered with graphene. In such a case, the device achieves 88.45 GHz at 17.5 fJ/bit.

Table 3 compares the main previously reported works in terms of performance and key features such as bandwidth, footprint, power consumption, FOM, and active area. The goal of the analysis carried out here is to investigate the impact of graphene's variation on the device's design including the power consumption whilst keeping a reasonable modulation bandwidth and

OPTICS CONTINUUM

footprint. Some previous devices have shown different performance and they suffer from either larger active area, footprint, or power consumption. It can be seen that our newly proposed device has the smallest active area. Also, the latter achieves excellent levels of power consumption (4.6 fJ/bit) and bandwidth (42.6 GHz) specially when bearing in mind that this device has only 25% of its ring covered with graphene whilst the others use 100%.

6. Conclusions

In this paper, we report a comprehensive analysis of an optical modulator composed of graphene. The ring resonator based-modulator has 2 layers of graphene. For power consumption analysis, the percentage of graphene was varied from 25% to 100% with 4 discrete steps of 25%. The device design and operation principle have been presented and explained. The values of the critical coupling condition (OFF-state) and 3-dB transmission (ON-state) are obtained. In addition, the main parameters of the graphene modulator are extracted based on transmission characteristics by using the finite element technique. Numerical results show the modulator consumes as low as 4.6 fJ/bit operating at 42.6 GHz with 25% of graphene. Alternatively, the modulator can operate at 88.45 GHz at the expense of consuming more energy per bit (17.5 fJ/bit) with 100% of graphene. The newly proposed 42.6 GHz modulator uses only 25% of the graphene when compared to currently reported graphene modulators for the ring resonator design. This means a significant reduction in the overall cost of the device i.e., the 25% graphene modulator is 4-fold cheaper than the 100% graphene modulator. The footprint and active area limits of the 42.6 GHz modulator as 22.1 μm^2 and 1.68 μm^2, respectively. To the best of our knowledge, this is the smallest active area to date. The modulator has an extremally compact footprint and the smallest active area, due to the reduced ring area with using 25% of graphene. The leverage of graphene as a green technology may become more substantial during the upcoming decade for ICT solutions, including mobile fronthaul, telecom, and datacom.

Funding. Conselho Nacional de Desenvolvimento Científico e Tecnológico; Coordenação de Aperfeiçoamento de Pessoal de Nível Superior.

Acknowledgments. None

Disclosures. The authors declare no conflicts of interest.

Data availability. Data underlying the results presented in this paper are not publicly available at this time based on data protection policy but may be obtained from the authors via e-mail upon reasonable request.

References

1. D. Littmann, C. Wigginton, P. Wílson, B. Haan, and J. Fritz, "Communications Infrastructure Upgrade: The Need for Deep Fiber," (2017).
2. T. R. Raddo, S. Rommel, B. Cimoli, and I. T. Monroy, "*The optical fiber and mmwave wireless convergence for 5G fronthaul networks*," in (IEEE, 2019), pp. 607–612.
3. T. R. Raddo, S. Rommel, B. Cimoli, C. Vagionas, D. Perez-Galacho, E. Pikasis, E. Grivas, K. Ntontin, M. Katsikis, D. Kritharidis, E. Ruggeri, I. Spaleniak, M. Dubov, D. Klonidis, G. Kalfas, S. Sales, N. Pleros, and I. Tafur Monroy, "Transition technologies towards 6G networks," *EURASIP Journal on Wireless Communications and Networking 2021*, 100 (2021).
4. M. Aldossary and H. A. Alharbi, "Towards a green approach for minimizing carbon emissions in fog-cloud architecture," IEEE Access **9**, 131720–131732 (2021).
5. Z. Niu, "Green communication and networking: A new horizon," IEEE Trans. on Green Commun. Netw. **4**(3), 629–630 (2020).
6. X. Dong, T. El-Gorashi, and J. M. Elmirghani, "IP over WDM networks employing renewable energy sources," J. Lightwave Technol. **29**(1), 3–14 (2011).
7. F. Bonaccorso, Z. Sun, T. Hasan, and A. C. Ferrari, "Graphene photonics and optoelectronics," Nat. Photonics **4**(9), 611–622 (2010).
8. J. Liu, Z. U. Khan, C. Wang, H. Zhang, and S. Sarjoghian, "Review of graphene modulators from the low to the high figure of merits," J. Phys. D: Appl. Phys. **53**(23), 233002 (2020).
9. M. Liu, X. Yin, E. Ulin-Avila, B. Geng, T. Zentgraf, L. Ju, F. Wang, and X. Zhang, "A graphene-based broadband optical modulator," Nature **474**(7349), 64–67 (2011).

OPTICS CONTINUUM

10. S. Ojaghi, S. Golmohammadi, and H. Soofi, "All-optical graphene-on-silicon slot waveguide modulator based on graphene's Kerr effect," Appl. Opt. **60**(26), 7945–7954 (2021).
11. J. Liu, Z. U. Khan, and S. Sarjoghian, "Suspended graphene double-layer modulator with an ultrahigh figure of merit and a subwavelength-thickness modulator with leaky mode," Appl. Opt. **58**(14), 3729 (2019).
12. S. J. Koester and M. Li, "High-speed waveguide-coupled graphene-on-graphene optical modulators," Appl. Phys. Lett. **100**(17), 171107 (2012).
13. M. Midrio, S. Boscolo, M. Moresco, M. Romagnoli, C. De Angelis, A. Locatelli, and A.-D. Capobianco, "Graphene–assisted critically–coupled optical ring modulator," Opt. Express **20**(21), 23144–23155 (2012).
14. M. R. Jalali Azizpour, M. Soroosh, N. Dalvand, and Y. Seifi-Kavian, "All-Optical Ultra-Fast Graphene-Photonic Crystal Switch," Crystals **9**(9), 461 (2019).
15. L. Wu, H. Liu, J. Li, S. Wang, S. Qu, and L. Dong, "A 130 GHz Electro-Optic Ring Modulator with Double-Layer Graphene," Crystals **7**(3), 65 (2017).
16. F. Zhou and W. Du, "Ultrafast all-optical plasmonic graphene modulator," Appl. Opt. **57**(23), 6645–6650 (2018).
17. Z. Wu and Y. Xu, "Design of a graphene-based dual-slot hybrid plasmonic electro-absorption modulator with high-modulation efficiency and broad optical bandwidth for on-chip communication," Appl. Opt. **57**(12), 3260–3267 (2018).
18. I. Chakraborty, K. Debnath, and V. Dixit, "Low-energy high-speed graphene modulator for on-chip communication," OSA Continuum **2**(4), 1273–1284 (2019).
19. M. AlAloul and M. Rasras, "Low Insertion Loss Plasmon-Enhanced Graphene All-Optical Modulator," ACS Omega **6**(11), 7576–7584 (2021).
20. K. Y. Lau, A. P. Perros, D. Li, M. Kim, and Z. Sun, "Scalable graphene electro–optical modulators for all-fibre pulsed lasers," Nanoscale **13**(21), 9873–9880 (2021).
21. B. S. Lee, B. Kim, A. P. Freitas, A. Mohanty, Y. Zhu, G. R. Bhatt, J. Hone, and M. Lipson, "High-performance integrated graphene electro-optic modulator at cryogenic temperature," Nanophotonics **10**(1), 99–104 (2020).
22. D. M. Neves and J. B. Silva, "Comparative study of energy and footprint minimization limit for two types of graphene-assisted ring-shape modulators," Opt. Quantum Electron. **51**(8), 280 (2019).
23. C. T. Phare, Y.-H. D. Lee, J. Cardenas, and M. Lipson, "Graphene electro-optic modulator with 30 GHz bandwidth," Nat. Photonics **9**(8), 511–514 (2015).
24. M. Liu, X. Yin, and X. Zhang, "Double-layer graphene optical modulator," Nano Lett. **12**(3), 1482–1485 (2012).
25. V. Sorianello, M. Midrio, G. Contestabile, I. Asselberghs, J. Van Campenhout, C. Huyghebaert, I. Goykhman, A. K. Ott, A. C. Ferrari, and M. Romagnoli, "Graphene–silicon phase modulators with gigahertz bandwidth," Nat. Photonics **12**(1), 40–44 (2018).
26. Y. Ding, X. Zhu, S. Xiao, H. Hu, L. H. Frandsen, N. A. Mortensen, and K. Yvind, "Effective electro-optical modulation with high extinction ratio by a graphene–silicon microring resonator," Nano Lett. **15**(7), 4393–4400 (2015).
27. C. Qiu, W. Gao, R. Vajtai, P. M. Ajayan, J. Kono, and Q. Xu, "Efficient modulation of 1.55 μm radiation with gated graphene on a silicon microring resonator," Nano Lett. **14**(12), 6811–6815 (2014).
28. H. Dalir, Y. Xia, Y. Wang, and X. Zhang, "Athermal broadband graphene optical modulator with 35 GHz speed," ACS Photonics **3**(9), 1564–1568 (2016).
29. D. Shekhawat and R. Mehra, "Design of Ultra-Compact and Highly-Sensitive Graphene Assisted Silicon Micro-Ring Resonator Modulator for Switching Applications," Silicon 1–8 (2021).
30. C. Zhong, J. Li, and H. Lin, "Graphene-based all-optical modulators," Front. Optoelectron. **13**(2), 114–128 (2020).
31. B.-H. Huang, W.-B. Lu, X.-B. Li, J. Wang, and Z. Liu, "Waveguide-coupled hybrid plasmonic modulator based on graphene," Appl. Opt. **55**(21), 5598–5602 (2016).
32. G. W. Hanson, "Dyadic Green's functions and guided surface waves for a surface conductivity model of graphene," J. Appl. Phys. **103**(6), 064302 (2008).
33. A. Yariv, "Critical coupling and its control in optical waveguide-ring resonator systems," IEEE Photonics Technol. Lett. **14**(4), 483–485 (2002).
34. Z. Cheng, H. K. Tsang, X. Wang, K. Xu, and J.-B. Xu, "In-plane optical absorption and free carrier absorption in graphene-on-silicon waveguides," IEEE J. Sel. Top. Quantum Electron. **20**(1), 43–48 (2014).
35. C. D. Salzberg and J. J. Villa, "Infrared refractive indexes of silicon germanium and modified selenium glass," J. Opt. Soc. Am. **47**(3), 244–246 (1957).
36. I. H. Malitson, "Interspecimen comparison of the refractive index of fused silica," J. Opt. Soc. Am. **55**(10), 1205–1209 (1965).
37. M. J. Dodge, I. H. Malitson, and A. I. Mahan, "A Special Method for Precise Refractive Index," Appl. Opt. **8**(8), 1703 (1969).
38. M. A. Giambra, V. Sorianello, V. Miseikis, S. Marconi, A. Montanaro, P. Galli, S. Pezzini, C. Coletti, and M. Romagnoli, "High-speed double layer graphene electro-absorption modulator on SOI waveguide," Opt. Express **27**(15), 20145 (2019).
39. W. Bogaerts, P. De Heyn, T. Van Vaerenbergh, K. De Vos, S. Kumar Selvaraja, T. Claes, P. Dumon, P. Bienstman, D. Van Thourhout, and R. Baets, "Silicon microring resonators," Laser Photonics Rev. **6**(1), 47–73 (2012).
40. R. Amin, Z. Ma, R. Maiti, S. Khan, J. B. Khurgin, H. Dalir, and V. J. Sorger, "Attojoule-efficient graphene optical modulators," Appl. Opt. **57**(18), D130–D140 (2018).

OPTICS CONTINUUM

41. J. S. Gomez-Diaz, C. Moldovan, S. Capdevila, J. Romeu, L. S. Bernard, A. Magrez, A. M. Ionescu, and J. Perruisseau-Carrier, "Self-biased reconfigurable graphene stacks for terahertz plasmonics," Nat Commun **6**(1), 6334 (2015).
42. Z. Qian, D. Yang, and W. Wang, "Terahertz modulation based on surface plasmon resonance by self-gated graphene," Opt. Commun. **414**, 52–58 (2018).
43. J. Gosciniak and D. T. H. Tan, "Theoretical investigation of graphene-based photonic modulators," Sci Rep **3**(1), 1897 (2013).
44. S. Qu, C. Ma, S. Wang, H. Liu, and L. Dong, "Modulation speed limits of a graphene-based modulator," Opt. Quantum Electron. **50**(1), 1–11 (2018).
45. M. Fan, H. Yang, P. Zheng, G. Hu, B. Yun, and Y. Cui, "Multilayer graphene electro-absorption optical modulator based on double-stripe silicon nitride waveguide," Opt. Express **25**(18), 21619–21629 (2017).